Cylindrical Misalignment Insensitive Wireless Power Transfer Systems

Daerhan Liu, *Student Member, IEEE* and Stavros V. Georgakopoulos, *Senior Member, IEEE*

***Abstract*—The widely used wireless power transfer method known as inductive coupling, suffers from dramatic efficiency drops; even over short distances. Strongly coupled magnetic resonance (SCMR) was introduced recently, and can achieve high efficiency at larger distances when compared to inductive coupling. However, standard SCMR systems are highly sensitive to the alignment between the transmitter and receiver, which is an issue that has limited their application in practical wireless powering systems. This paper proposes a new SCMR-based topology that can maintain a constant high efficiency through 360° of misalignment. Specifically, a cylindrical geometry is proposed for the SCMR transmitter instead of using planar loops. Two types of materials are used: copper wire and flexible PCB, and their performances are compared and studied. This new system is able to achieve efficiency above 40% for the entire 360° misalignment without null points, and for the majority of angles the efficiencies stay at 70%. In addition, this new system is wearable and can be used as a portable wireless powering device.**

***Index Terms*—Cylindrical topology, misalignment insensitive, strongly coupled magnetic resonance (SCMR), wireless power transfer.**

I. Introduction

WIRELESS power transfer (WPT) methods have taken a more important role in our everyday life. Inductive coupling has been used in various practical applications, such as electric vehicles [1], RFID [2], [3], implanted medical devices (IMDs) [4], and mobile devices [5]. However, inductive coupling has several disadvantages, such as low transmitting efficiency and short transmitting range. Strongly coupled magnetic resonance (SCMR) is a new WPT method that has been recently developed and provides greater efficiency at longer range compared to traditional near-field WPT methods [6]–[8]. In order for SCMR to achieve high efficiency, it requires that the transmitting (TX) and receiving (RX) elements (typically loops or coils) are designed so that they resonate at the frequency where the elements naturally exhibit maximum Q-factor [9].

Manuscript received March 21, 2017; revised June 26, 2017, September 8, 2017, and November 18, 2017; accepted December 27, 2017. Date of publication January 8, 2018; date of current version August 7, 2018. This work was supported by the Air Force Office of Scientific Research under grant FA9550-16-1-0145. Recommended for publication by Associate Editor O. C. Onar. *(Corresponding author: Stavros V. Georgakopoulos.)*

The authors are with the Department of Electrical and Computer Engineering, Florida International University, Miami, FL 33174 USA (e-mail: ddaer001@fiu.edu; georgako@fiu.edu).

Color versions of one or more of the figures in this paper are available online at http://ieeexplore.ieee.org.

Digital Object Identifier 10.1109/TPEL.2018.2791350

Even though SCMR exhibits higher efficiency than inductive coupling, its performance is highly sensitive to the alignment between the transmitter and receiver elements. An optimization technique for improving the efficiency of SCMR systems under lateral misalignment was presented in [10]. Specifically, 48.4% efficiency was achieved by using an adaptive matching network. However, no solution for angular misalignment was proposed in [10]. Also, the effects of few misalignment angles on SCMR's efficiency were examined in [11] and [12]. However, the main focus of [11] and [12] was to study multiple transmitter/receiver WPT systems and their misalignment analysis was very limited. Analytical formulations for the power transfer efficiency of inductive links under lateral and angular coil misalignment were presented in [13]. Two novel SCMR topologies were proposed in [14] but their efficiency was only studied for a maximum angular misalignment of 90°. Furthermore, analytical models for SCMR that incorporate misalignment effects were presented in [15]. SCMR's radial and angular misalignment sensitivity were examined by [16] and [17], respectively. SCMR's angular misalignment sensitivity was decreased through the use of tuning circuits but high efficiency was not achieved above 60° of misalignment rotation. An omnidirectional WPT method that utilizes current phase shifting between power inputs was studied in [18]. However, the requirement of different current control in three separated source loops can be difficult to implement in practice. Further investigation of this method can also be found in [19]. Angular misalignment was also examined in [20] that reconfigured the WPT system using switching between different-size source loops and load loops thereby increasing the complexity of the WPT system and making its practical implementation difficult. A new misalignment insensitive SCMR system, which exhibits no nulls in power transfer efficiency in the azimuth plane, was presented in [21]. However, such a system requires three-dimensional (3-D) elements for both transmitter and receiver, which in some applications cannot be easily implemented. This paper proposes new SCMR structures that are less sensitive to misalignment compared to standard SCMR systems.

II. SCMR Theory and Design

A standard SCMR system is shown in Fig. 1 and it consists of the following: (a) a transmitter with one source loop, where the excitation is connected, and a TX resonator coil or loop, and (b) a receiver with one load loop, where the load is connected, and an RX resonator coil or loop. In order for SCMR to achieve high WPT efficiency, the TX and RX resonators must resonate

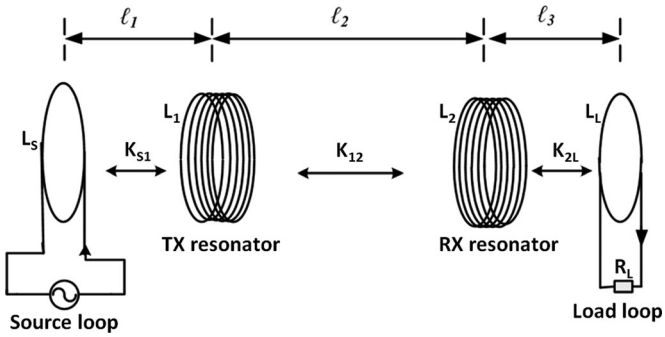

Fig. 1. Schematic of standard SCMR system.

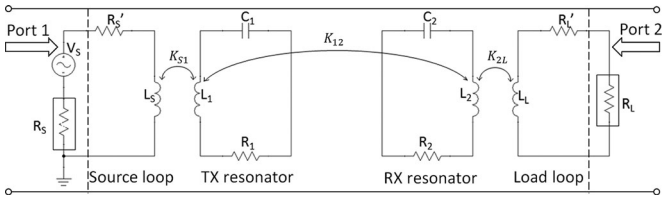

Fig. 2. Equivalent circuit of an SCMR system.

at the same frequency, which is also the frequency where the resonators naturally exhibit the highest Q-factor. It is this condition indeed that enables SCMR to achieve WPT efficiencies that are significantly greater than inductively coupled or resonant inductively coupled systems. This has been confirmed in [22] where three types of WPT systems of the same size and operating frequency were compared, namely:

1) A nonresonant inductively coupled system,
2) A resonant inductively coupled system, and
3) An SCMR system.

The equivalent circuit of an SCMR system is shown in Fig. 2. In Fig. 2, R_S and R_L are the internal resistances of the input and output ports, respectively; R'_S, R_1, R_2, and R'_L are the total resistances of the source loop, TX resonator, RX resonator, and load loop, respectively; L_S, L_1, L_2, and L_L are the corresponding inductances of these loops; C_1 and C_2 are the external capacitors connected to the TX and RX resonator loops, respectively; K_{S1}, K_{12}, and K_{2L} are the coupling coefficients between the loops. The input and output ports are shown in Fig. 2 as port 1 and port 2, respectively. The source loop delivers power to the TX resonator through inductive coupling, and the RX resonator delivers power to the load loop through inductive coupling. Then, the TX resonator efficiently transfers power to the RX resonator over large distances by satisfying the SCMR condition (i.e., both TX and RX resonators resonate at the same frequency, where their Q-factor is naturally maximum). The size of the resonators of an SCMR system is determined by the frequency where the Q-factor is maximum. The frequency where the Q-factor of a loop is maximum can be written as [23]

$$f_{\max} = \frac{c^{8/7}\mu_0^{1/7}\rho^{1/7}}{4 \cdot 15^{2/7}\pi^{11/7}r_c^{2/7}r^{6/7}} \tag{1}$$

where μ_0 is the permeability of free space, ρ is the loop's material resistivity, r_c is the cross-sectional radius of the loop, and r is the radius of the loop. In order to design a proper SCMR system that operates at a certain frequency, f_0, with high efficiency, the following equation must be satisfied:

$$f_0 = f_{\max}. \tag{2}$$

Based on (1) and (2), the radii of the TX and RX resonator loops are equal to

$$r = \frac{c^{4/3}\mu_0^{1/6}\rho^{1/6}}{4^{7/6}15^{1/3}\pi^{11/6}r_c^{1/3}f_0^{7/6}} \tag{3}$$

In order to form resonant TX and RX loops, a lumped capacitor must be connected on each of these loops. This capacitor can be calculated using the following formula:

$$L = \mu_0 r\left[\ln\left(\frac{8r}{r_c}\right) - 2\right] \tag{4}$$

$$C = \frac{1}{(2\pi f_{\max})^2 L} \tag{5}$$

where L is the equivalent inductance of each TX and RX loop. Therefore, the TX/RX resonators can be designed using (2)–(5). The source and load coils in all of our designs are scaled versions (i.e., have same geometrical shape) of the TX and RX resonator coils. Therefore, the scaling factor that scales the TX (or RX) resonator coil to the source (or load) resonator coil is the only parameter that needs to be determined once the TX and RX resonators are designed. ANSYS HFSS is used to optimize this scaling factor in order to achieve optimal power transfer efficiency. Based on our design experience and simulation results, the size of the source and load coils is typically 1/2 to 3/5 of the resonator size. It has been shown by several papers [7], [17] that the typical distance at which an SCMR system exhibits maximum efficiency is approximately equal to the diameter of the TX and RX resonators.

III. Misalignment Analysis

Standard SCMR systems exhibit high sensitivity to angular misalignment, and they have been studied in several papers [17], [24]–[26]. Specifically, in [17] frequency tuning is applied and a nearly constant efficiency at approximately 75% was obtained until the receiver is rotated past 60°. Beyond 60°, the efficiency drops rapidly to zero from 60° to 90° misalignment. In [26], it was shown that the efficiencies vary from 40% to 20% from 0° to 45° misalignment angle, and from 20% to 0% from 45° to 90° misalignment angle. In this paper, the misalignment analysis of conformal SCMR (CSCMR) systems is investigated. Conventional CSCMR systems are constructed so that the source and load loops are embedded into the TX and RX resonators, respectively, which make the TX and RX elements planar [27], as shown in Fig. 3. Also, Fig. 3 illustrates the definition of the azimuth misalignment angle for our study. Azimuth misalignment sensitivity examines how the efficiency of an SCMR system changes when the RX element (load loop and RX resonator) rotates around the TX element (source loop and TX resonator) in the xy plane (i.e., rotates around the z-axis from $\varphi = 0°$ to 360°), while the TX element is fixed. It should be noted that due to the reciprocity theorem [28], the effect of rotating the TX element around the RX element is the same with rotating the

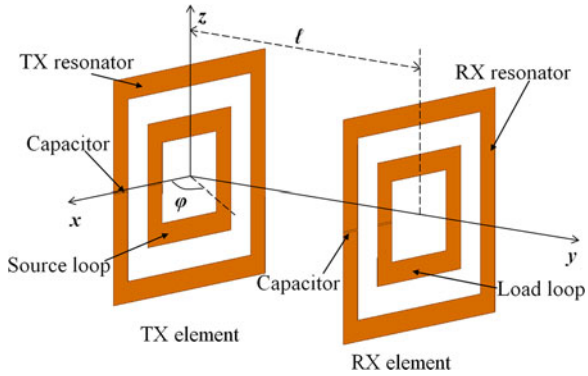

Fig. 3. SCMR system illustrating azimuth angular misalignment.

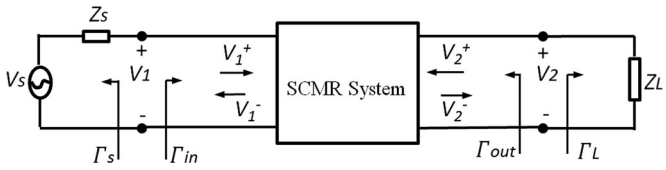

Fig. 4. Two-port network for SCMR system with source and load impedance.

RX element around the TX element. In what follows, the azimuth misalignment sensitivities for all the SCMR systems will be examined. All the simulations in this paper were performed using ANSYS HFSS [29] and ANSYS Designer [30]. The load loops of all the designs examined here are connected to 50 Ω loads. All CSCMR resonators examined below were designed to resonate at the frequency where their Q-factor is maximum, which was accomplished by using analytical equations and simulations. All the SCMR systems presented here were designed to operate at the 27.12 MHz ISM band.

In order to quantify SCMR system power transfer efficiency, the transducer power gain is used since it accounts for both source and load mismatches. The transducer power gain is defined as the ratio of power delivered to the load to the power available from the source. The entire SCMR WPT system is considered as a two-port network. In order to better understand the power gain definition, this two-port network with source and load impedance is shown in Fig. 4.

The transducer power gain can be defined in terms of S-parameters per [31] as follows:

$$G_T = \frac{P_L}{P_{\text{avs}}} = \frac{|S_{21}|^2 \left(1-|\Gamma_S|^2\right)\left(1-|\Gamma_L|^2\right)}{|1-\Gamma_S\Gamma_{\text{in}}|^2|1-S_{22}\Gamma_L|^2} \tag{6}$$

where P_L is the power delivered to the load, and P_{avs} is the power available from the source. With reference to Fig. 4, the reflection coefficient seen looking toward the source is

$$\Gamma_S = \frac{Z_S - Z_0}{Z_S + Z_0} \tag{7}$$

while the reflection coefficient seen looking toward the load is

$$\Gamma_L = \frac{Z_L - Z_0}{Z_L + Z_0} \tag{8}$$

where Z_0 is the characteristic impedance reference for the scattering parameters of the two-port network. The mismatch

TABLE I
CONVERSION OF S-PARAMETERS TO Z-PARAMETERS

$\boldsymbol{Z}_{11}$	$Z_0 \frac{(1+S_{11})(1-S_{22})+S_{12}S_{21}}{(1-S_{11})(1-S_{22})-S_{12}S_{21}}$
$\boldsymbol{Z}_{12}$	$Z_0 \frac{2S_{12}}{(1-S_{11})(1-S_{22})-S_{12}S_{21}}$
$\boldsymbol{Z}_{21}$	$Z_0 \frac{2S_{21}}{(1-S_{11})(1-S_{22})-S_{12}S_{21}}$
$\boldsymbol{Z}_{22}$	$Z_0 \frac{(1-S_{11})(1+S_{22})+S_{12}S_{21}}{(1-S_{11})(1-S_{22})-S_{12}S_{21}}$

Z_0 is the reference impedance

corresponding to the input impedance of the terminated two-port network is given by the reflection coefficient Γ_{in}, and it is defined as

$$\Gamma_{\text{in}} = S_{11} + \frac{S_{12}S_{21}\Gamma_L}{1-S_{22}\Gamma_L}. \tag{9}$$

We assume in all our designs that the source and load impedances are 50 Ω, which, according to (7) and (8), makes $\Gamma_s = \Gamma_L = 0$, and reduces (6) to $G_T = |S_{21}|^2$. Therefore, in this paper, the power transfer efficiency, η, of all our designs is equal to G_T and it is defined as

$$\eta = |S_{21}|^2. \tag{10}$$

The efficiency of our prototypes is measured using a vector network analyzer and it is based on the S-parameters. Specifically, ports 1 and 2 of the network analyzer are connected to the transmitter and receiver, respectively, and the S-parameters are measured. Then, the data of the measured efficiency is calculated by directly programming the equation $|\mathrm{S}_{21}|^2$ on the network analyzer.

In this paper, we assume the input and output impedances are matched to 50 Ω. However, in certain cases, the input and output impedances may not be 50 Ω. Some recent studies have provided insight on optimizing the total system efficiency that includes the effects of the power amplifier and rectifier [32], [33]. This paper concentrates on examining the misalignment performance of the proposed cylindrical systems. The optimization flow described in our paper including (1)–(5) is still consistent for imbalanced impedance situations since this flow derives designs that satisfy the fundamental condition for SCMR systems to exhibit maximum efficiency, i.e., the TX and RX resonators must resonate at the same frequency, which is also the frequency where the resonators naturally exhibit the highest Q-factor. In the case of imbalanced impedance, different approaches, which improve the performance of the entire system, can be followed. For example, a matching network can be used between the WPT elements and the amplifier and/or rectifier. Also, in cases where the designer chooses a reference impedance that is different than 50 Ω, the following process can be used to convert the measured and/or simulated S-parameters based on 50 Ω reference to another impedance. First, convert the S-parameters based on 50 Ω reference ($Z_0 = 50\,\Omega$) to Z-parameters using the equations shown in Table I. Second, set Z_0 to the new reference impedance and convert the Z-parameters to the new S-parameters for the new reference impedance using the equations shown in Table II [31].

TABLE II
CONVERSION OF *Z*-PARAMETERS TO *S*-PARAMETERS

S_{11}	$\frac{(Z_{11}-Z_0)(Z_{22}+Z_0)-Z_{12}Z_{21}}{\Delta Z}$
S_{12}	$\frac{2Z_{12}Z_0}{\Delta Z}$
S_{21}	$\frac{2Z_{21}Z_0}{\Delta Z}$
S_{22}	$\frac{(Z_{11}+Z_0)(Z_{22}-Z_0)-Z_{12}Z_{21}}{\Delta Z}$

$\Delta Z = (Z_{11}+Z_0)(Z_{22}+Z_0) - Z_{12}Z_{21}$
Z_0 is the reference impedance

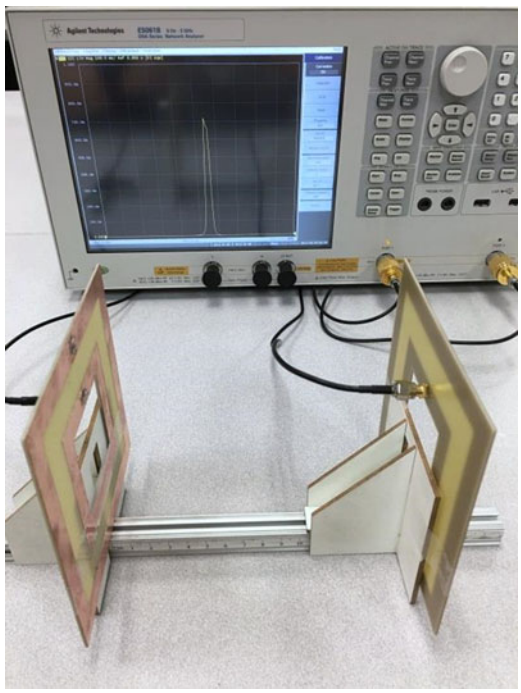

Fig. 5. Measurement setup of conventional CSCMR for 180° of misalignment.

A. Conformal SCMR

First, the misalignment sensitivity of a CSCMR system is studied here. In a conventional CSCMR system, the source loop and load loop are embedded into the TX and RX resonators, respectively. Therefore, the source loop is coplanar with the TX resonator and the load loop is coplanar with the RX resonator (see Fig. 3). This topology is completely planar and saves a lot of space in practical implementations, whereas standard SCMR requires the source loop and TX resonator to be separated, as well as the RX resonator and load loop. For standard SCMR systems, the TX and RX resonators must be placed between the source and load loops which make their performance very sensitive to misalignment, as was discussed in [21]. The conventional CSCMR elements can be either circular or rectangular. All our designs in this paper use rectangular elements.

A conventional CSCMR system is designed (see Fig. 5) under the design guidelines presented in section II with the following specifications. The TX and RX resonators (outside loops) are squares with lengths of 115 mm. The source and load loops are squares with lengths of 57.5 mm (half the size of the resonators).

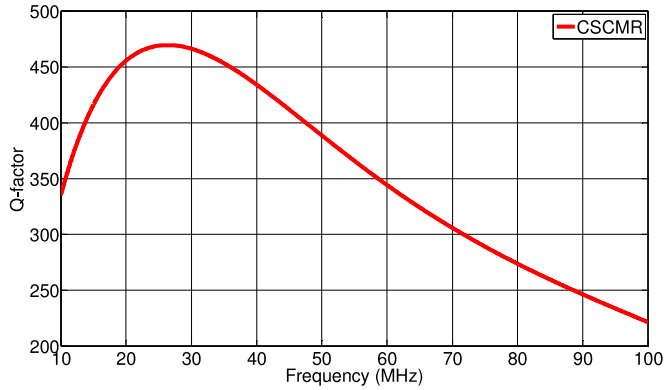

Fig. 6. Simulated *Q*-factor of elements of conventional CSCMR system.

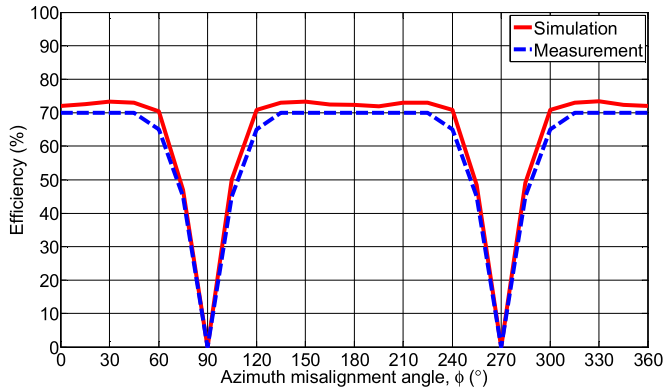

Fig. 7. Misalignment results of conventional conformal SCMR.

The trace of all the square loops is 12-mm wide and 0.035-mm thick copper. The distance between the TX and RX elements is 150 mm, which was optimized through simulations. Since the TX and RX elements are identical in this case, the *Q*-factors of both elements are also the same. As shown in Fig. 6, this system's *Q*-factor naturally exhibits its maximum at 27.12 MHz. The capacitors used on both resonators are 139 pF. The operating frequency of this system is 27.12 MHz.

Fig. 7 plots the efficiency of this conventional CSCMR system versus the azimuth misalignment angle between the transmitter and receiver. It shows that the efficiency stays approximately 70% for misalignment angles of 0° to 60°, 120° to 240° and 300° to 360°. Also, since no magnetic flux can be coupled when the transmitter is perpendicular to the receiver, the efficiency drops from 70% to 0% from 60° to 90°, 120° to 90°, 240° to 270°, and 300° to 270°. Our goal in this paper, is to develop SCMR systems that do not exhibit nulls in their efficiency for any angle of azimuth misalignment. These designs will be presented in the following sections.

B. Cylindrical SCMR Based on Wire Elements

A new SCMR system is proposed here, and it is shown in Fig. 8. In this system, the TX element is a 3-D cylindrical wire structure (see Fig. 8) and it is proposed for the first time here. Also, this system uses a receiver with conventional CSCMR

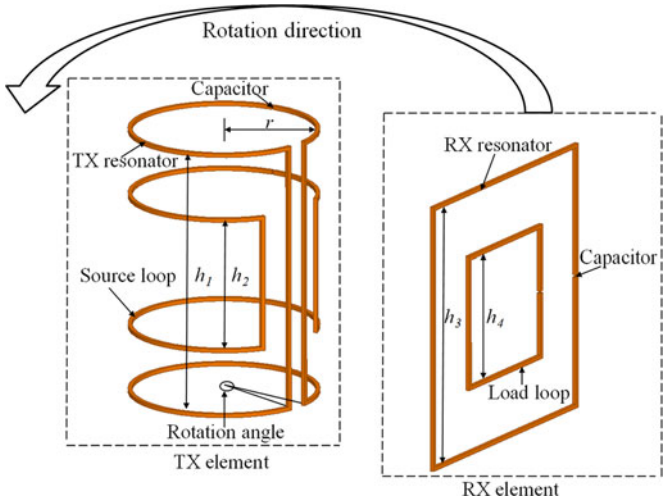

Fig. 8. Schematic of proposed cylindrical SCMR based on wire elements.

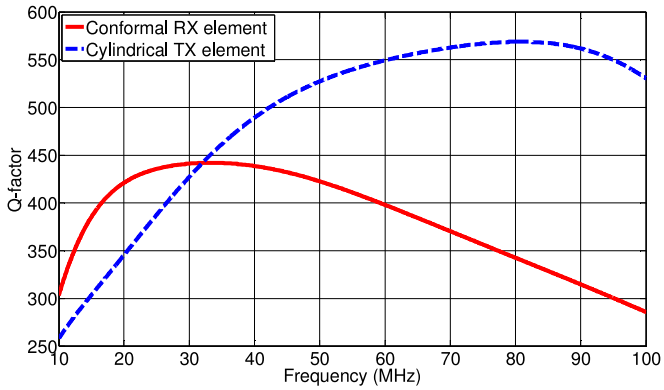

Fig. 9. Simulated Q-factor of elements of proposed cylindrical SCMR system based on wire elements.

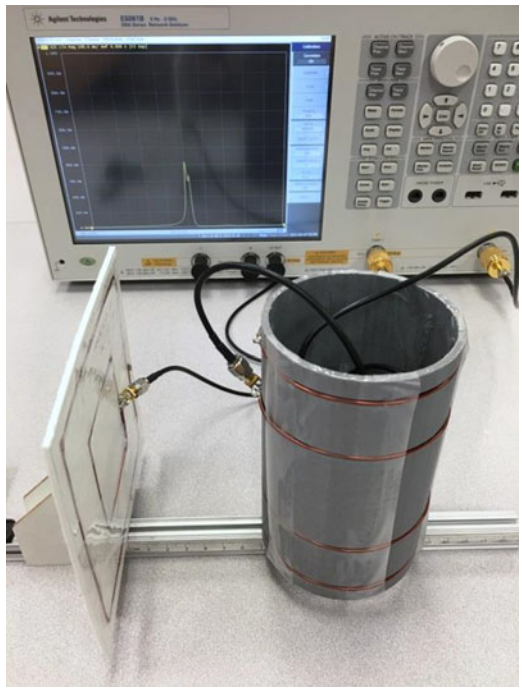

Fig. 10. Measurement setup of proposed cylindrical SCMR based on wire elements for 180° of misalignment.

elements (see Fig. 8). The source loop and TX resonator are designed so that they can wrap around a cylinder in order to create cylindrical symmetry for the transmitter thereby providing constant efficiency for the entire 360° of angular misalignment without any nulls. The rotation angle, which is illustrated in Fig. 8, is the angle spanned by the cylindrical source and TX resonator elements. The misalignment setup starts out at 0° when the conformal RX element is facing the gap of the TX element, as shown in Fig. 8. The misalignment rotation from 0° to 360° is defined as the RX element rotating around the TX element counterclockwise while keeping the same distance, as illustrated in Fig. 8 with the rotation direction arrow.

It should be pointed out that the geometries of the cylindrical elements are kept consistent with the geometry of the CSCMR design in terms of the heights of the source loop and TX resonator. This was done in order to have a fair comparison among all the designs, and to ensure that geometry differences do not contribute to differences in efficiency. Different geometrical parameters, such as height, radius, and cross-sectional radius of the cylindrical element can be optimized and their effect on the WPT performance can be studied. However, the main scope of this paper is to prove the misalignment insensitivity and high efficiency of this design. Therefore, the optimization of this design will be examined by our future work and in this paper, the parameters remain consistent for fair comparisons of the different systems. Fig. 9 illustrates the simulated Q-factors of the TX and RX elements of this system. The Q-factor of the conformal RX element exhibits its maximum at the desired frequency, but the cylindrical TX element does not. This is expected, since the geometries of the cylindrical elements are different from the geometries of the conformal elements.

A prototype of the proposed cylindrical SCMR based on copper wire is shown in Fig. 10. The radius of the cylindrical elements is $r = 40$ mm. The height of the TX resonator is $h_1 = 115$ mm. The height of the source loop is $h_2 = 57.5$ mm (half the size of the resonator). The cross-sectional radius of the copper wire is 1.7 mm. The rotation angle of the TX resonator is 345°. Our simulation analysis found that when the rotation angle of the source loop is equal to 8/9 of the TX resonator (which is 306.7°), maximum efficiency is achieved. Squared structures are used for the RX element and they are made using the same wire as the TX element with a cross-sectional radius of 1.7 mm. The length of the resonator is $h_3 = 115$ mm and the length of the load loop is $h_4 = 57.5$ mm (half the size of the resonator). The distance between the outer surface of TX elements and RX elements is 70 mm. The capacitors used on the TX and RX resonators are 82 pF and 100 pF, respectively. The operating frequency for this system is 27.12 MHz.

Fig. 11 illustrates the efficiency of the proposed cylindrical SCMR system for 360° of azimuth misalignment. It can be seen that the efficiency varies from 30% to 40% throughout the 360°

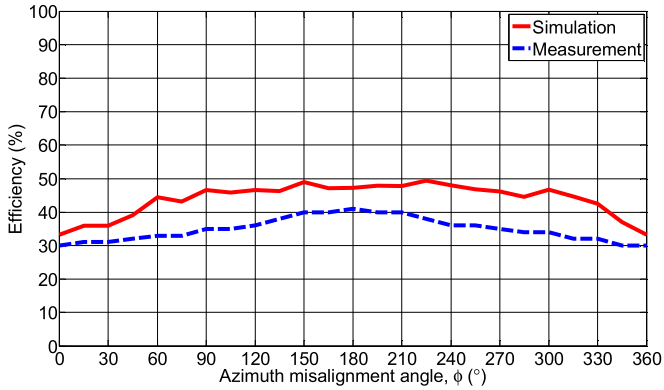

Fig. 11. Misalignment results of proposed cylindrical SCMR based on wire elements.

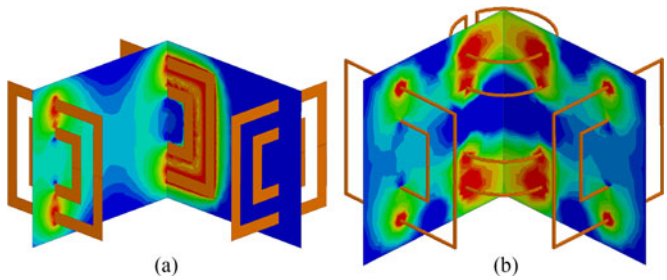

Fig. 12. Magnetic field generated by (a) conventional CSCMR and (b) proposed cylindrical SCMR.

misalignment rotation, also it exhibits no null for any angle, which solves the misalignment problem of CSCMR described above. This happens, because the proposed cylindrical SCMR TX elements generate a magnetic field that is symmetric around these elements. On the contrary, conventional CSCMR TX elements generate a magnetic field that has nulls at certain locations around these elements (at these null locations the conventional CSCMR TX and RX elements cannot couple yielding zero WPT efficiency). This is confirmed in Fig. 12 that compares the magnetic field distributions of conventional CSCMR and proposed cylindrical SCMR systems. Fig. 12 shows that in a conventional CSCMR system there is no coupling when the RX element is positioned perpendicularly to the TX element whereas in a proposed cylindrical SCMR system, there is coupling between the cylindrical TX element and the RX element for approximately 360° of azimuth misalignment. The slight difference between simulations and measurements in Fig. 11 can be attributed to capacitor losses. In the simulations capacitors are ideal, whereas in practice capacitors exhibit some loss. In our measurement setup, nonmagnetic, high-Q, low ESR (equivalent series resistance) ceramic capacitors are used with Q-factor above 1000 at our operating frequency of 27.12 MHz. Even though high-Q capacitors are used, they still exhibit small loss and this is the reason that the simulated and measured results are slightly different. This was also explained in [27].

Fig. 11 also shows that the efficiency of the proposed cylindrical SCMR system is smaller than the efficiency of the conventional CSCMR system (see Fig. 7) for most azimuth misalignment angles. This occurs because the copper wire that

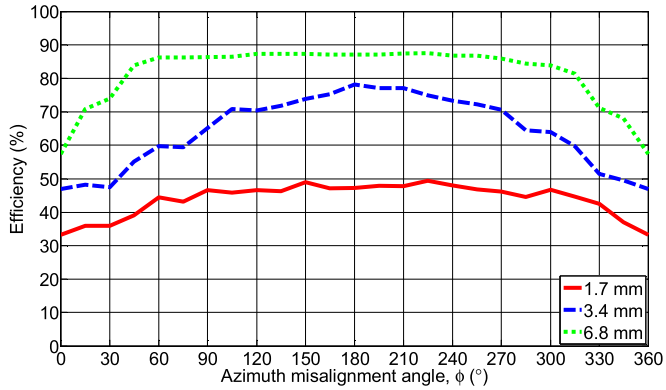

Fig. 13. Simulated results of three proposed cylindrical SCMR systems based on wire elements with different cross-sectional radii.

is used has small cross-sectional radius. According to [28]

$$R = \frac{l}{P} R_S = \frac{l}{P}\sqrt{\frac{\omega\mu_0}{2\sigma}} \tag{11}$$

where R is the dc resistance of the copper loop, l is the length of the copper wire, P is the perimeter of the cross section of the wire, R_S is the conductor surface resistance, ω is the angular frequency, μ_0 is the permeability of free space, and σ is the conductivity of the metal. According to (11), the dc resistance of the cylindrical system based on copper wire is 0.5 Ω. Given that l does not change once the geometry of the model is decided and other parameters are all constant, the only parameter that affects the dc resistance is P, which in turn makes the cross-sectional radius of the copper wire the determining factor for R. The smaller the radius is, the higher the resistance of the loop, thereby the lower the efficiency. This is validated by comparing the simulated efficiency of three proposed cylindrical SCMR systems constructed by copper wire with different cross-sectional radii in Fig. 13. It can be concluded from Fig. 13, as expected, that the thicker the wire is, the higher the efficiency. Furthermore, thicker wire makes the gap between the edges of the cylinders smaller, which in turn results in higher starting and finishing efficiencies when rotating. However, given the difficulty in bending thick copper wire, it was not possible for us to manually manufacture the prototype with thicker copper wire and maintain the dimensional accuracy of the prototype compared to the simulated model.

C. Cylindrical SCMR With Flexible PCB

In this section, an improved design of proposed cylindrical SCMR is discussed, and it is shown in Fig. 14. This system uses flexible PCBs to construct the cylindrical elements of the transmitter instead of wires, which were used in the previous section. The flexible PCB consists of a bendable polyethylene (PTFE) substrate laminated with 0.035-mm thick copper. By using this material, the cylindrical elements can be easily fabricated by producing the flexible PCB to the desired size and shape, then wrapping it around a cylinder base made by a 3-D printer. This method does not only simplify our manufacturing process, but also generates a prototype that is accurately made

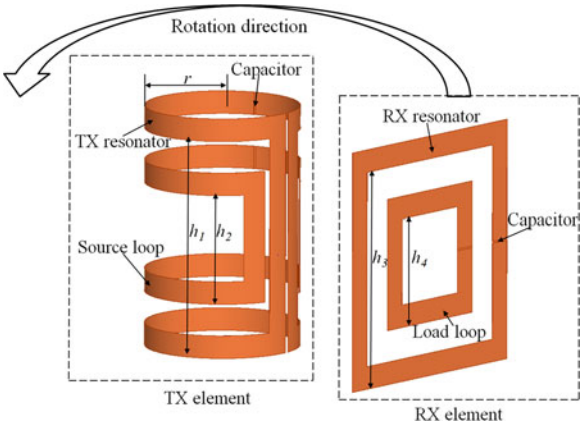

Fig. 14. Schematic of proposed cylindrical SCMR based on flexible PCB.

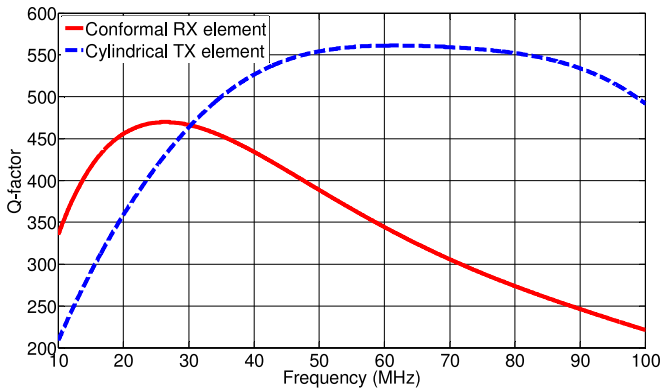

Fig. 15. Simulated Q-factor of elements of proposed cylindrical SCMR system with flexible PCB.

and has almost the same geometry with the simulation model. As shown in Fig. 15, the simulated Q-factors of the elements of the flexible PCB system are similar to the ones of the copper wire system, where the Q-factor of the conformal RX element naturally exhibits its maximum at 27.12 MHz and the Q-factor of the cylindrical element does not. The position demonstrated in Fig. 14 is considered 0° misalignment, where the gap of the TX element is facing the RX element. The process of misalignment rotation from 0° to 360° is defined as the RX element rotating around the TX element counterclockwise while keeping the same distance, as illustrated in Fig. 14 with the rotation direction arrow.

A flexible PCB cylindrical SCMR prototype is illustrated in Fig. 16 with the radii presented below. The radius of the cylindrical elements is $r = 40$ mm. The height of the TX resonator and source loop is $h_1 = 115$ mm and $h_2 = 57.5$ mm (half the size of the resonator). The rotation angle of the TX resonator is 340° and the rotation angle of the source loop is set as 7/8 of the TX resonator, i.e., 297.5°. These rotation angles were determined for optimal performance through simulation analysis. The squared RX elements have $h_3 = 115$ mm length for the resonator and $h_4 = 57.5$ mm (half the size of the resonator) length for the load loop. The flexible PCB used is 12 mm wide. The distance between the outer surface of TX elements and RX

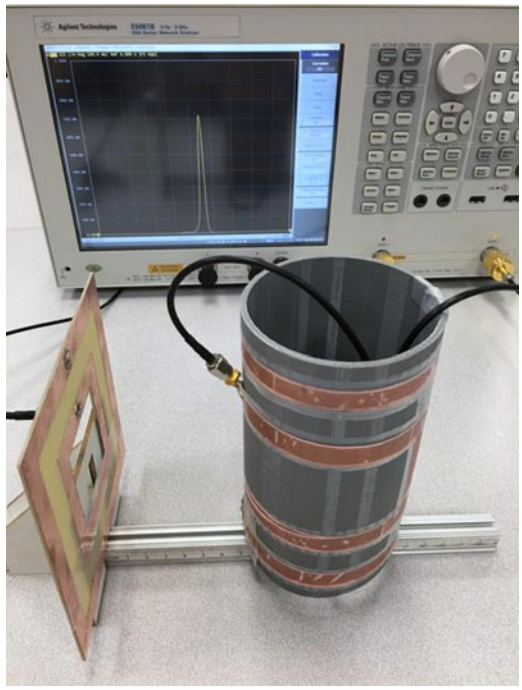

Fig. 16. Measurement setup of proposed cylindrical SCMR with flexible PCB for 180° of misalignment.

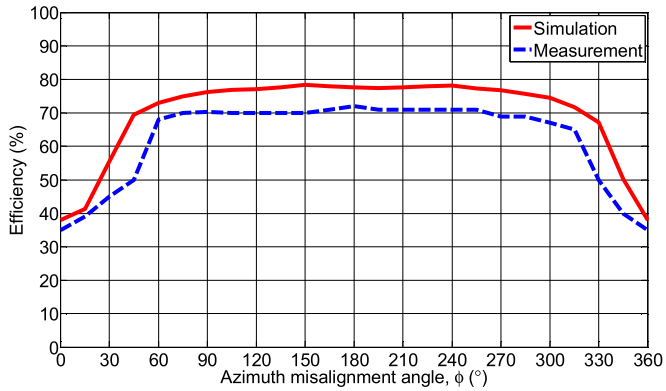

Fig. 17. Misalignment results of proposed flexible PCB cylindrical SCMR.

elements is 70 mm. The capacitors for the TX and RX resonators are 120 pF and 139 pF, respectively. The operating frequency is 27.12 MHz.

Fig. 17 shows the misalignment performance for the proposed flexible PCB cylindrical SCMR system. Since it has the same topology with the wire model discussed previously, no nulls were generated throughout the 360° misalignment rotation. This shows that the proposed cylindrical topology is indeed misalignment insensitive independently of the cross-section of the conductive traces. Also, the flexible PCB design achieves higher efficiencies. Specifically, the efficiency varies from 35% to 70% for 0° to 60°, and 270° to 360° misalignment angles. Then, the efficiency stays around 70% from 60° to 270° (measurement data) whereas for the efficiency of the wire model stayed at around 35% for all the angles. The smallest efficiency

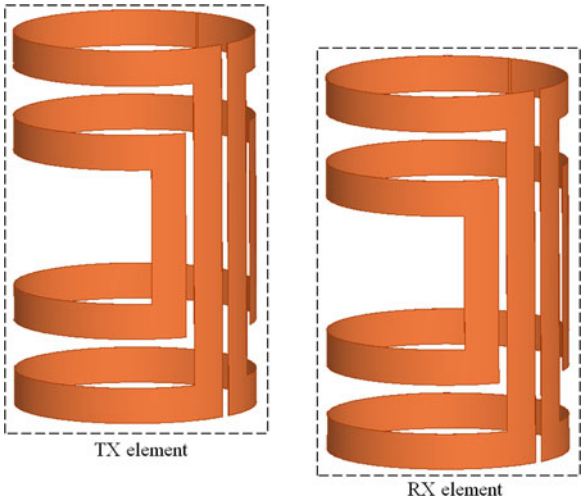

Fig. 18. Simulation model of flexible PCB cylindrical SCMR with cylindrical TX and RX elements.

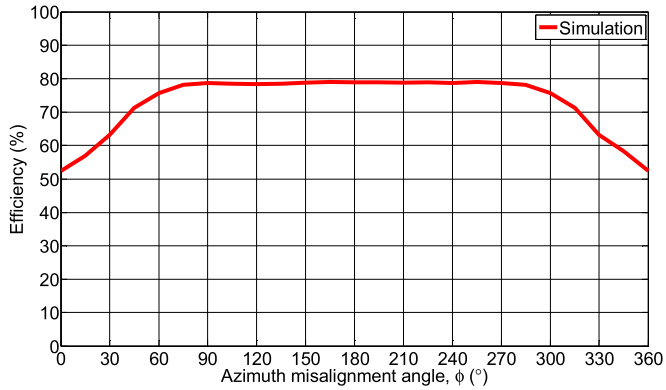

Fig. 19. Simulated misalignment result of flexible PCB cylindrical SCMR with cylindrical structures for both TX and RX elements.

occurs when the RX elements are at 0° and 360° misalignment angle. At these positions, less magnetic energy can be coupled between TX and RX since the gap of the cylindrical resonator is facing the conformal receiver. Even though the flexible PCB has much thinner trace than the copper wire, its ability to generate higher efficiency is still expected and this is explained in what follows. The main geometries of both systems (wire and flexible PCB systems) are the same and therefore, the total lengths of the copper wires and flexible PCB traces are the same. The electrical equivalent radius is shown in [28], and for a metal strip whose thickness is negligible, its equivalent circular cylinder radius is

$$a_e = 0.25a \tag{12}$$

where a is the width of the strip. In this case, the width of the flexible PCB is 12 mm, therefore, the equivalent radius is 3 mm. According to (11), it is obvious that with 0.14 Ω, the dc resistance of the flexible PCB model is much smaller than 0.5 Ω of the copper wire model, hence higher efficiency is achieved. The cylindrical structures of the source loop and TX resonator are not complete (do not cover 360° of rotation) and this explains the drop in efficiency for low and high angles of misalignment. In conclusion, the proposed flexible PCB cylindrical SCMR system provides misalignment insensitive performance and achieves large efficiencies for most angles.

To expand upon the results achieved above, the misalignment behavior of a SCMR system with both TX and RX elements being cylindrical, is examined here. Although it was discussed in Section I that it is not practical for certain applications to have both TX and RX elements be cylindrical, these results are presented for completeness. In the simulation setup, 0° misalignment is shown in Fig. 18 where the RX element is facing the gap of TX element. The distance between the outer surfaces of both elements is 50 mm, which is optimized from simulation to achieve highest efficiency. The smaller range of this SCMR system compared to the system of Fig. 14 is expected since this SCMR system is operating at a higher frequency. Since the geometry of the cylinder is different than the conformal SCMR, the frequency where its Q-factor exhibits its maximum is different, therefore, the operating frequency is changed. In this case, the maximum efficiency of the system occurs when the operating frequency is 90 MHz. The capacitors used on both TX and RX elements are 9 pF. The simulated efficiency for different misalignment angles is illustrated below in Fig. 19.

Fig. 19 shows that the SCMR system with both TX and RX elements cylindrical also exhibits no nulls in the misalignment setup, while achieving relatively high efficiencies. Specifically, the efficiency stays at around 78% from 75° to 285° misalignment angles, while varies from 52% to 78% from 0° to 75° and 285° to 360° misalignment angles. In conclusion, our results indicate that the cylindrical SCMR systems of Figs. 14 and 18 provide significantly less sensitivity to misalignment compared to standard SCMR and conventional CSCMR systems. Also, the cylindrical SCMR system of Fig. 14 will be more practical for most applications as it allows either the TX or the RX to be conformal.

D. Lateral Misalignment

In this section, the lateral misalignment performance comparison of conventional CSCMR and proposed cylindrical SCMR systems is presented. The cylindrical SCMR system with flexible PCB is chosen to be compared with CSCMR for the lateral misalignment for their same 12-mm width copper material and approximately 70% highest achievable efficiencies for both systems. The measurement setups for both systems are consistent with previous sections where the range for CSCMR is 150 mm and 70 mm for cylindrical SCMR. The misalignment angle for CSCMR is set at 0° and 180° for cylindrical SCMR for them to achieve maximum efficiencies. Figs. 20 and 21 illustrate the measured performance comparison between conventional CSCMR and proposed cylindrical SCMR with flexible PCB for x-axis and z-axis lateral misalignment, respectively. The x-axis and z-axis are defined in Fig. 3.

For the x-axis lateral misalignment (see Fig. 20), the efficiency of conventional CSCMR stays approximately constant at 70% from 0 to 7 cm of lateral misalignment and then gradually drops to almost zero from 7 to 18 cm of lateral misalignment. The

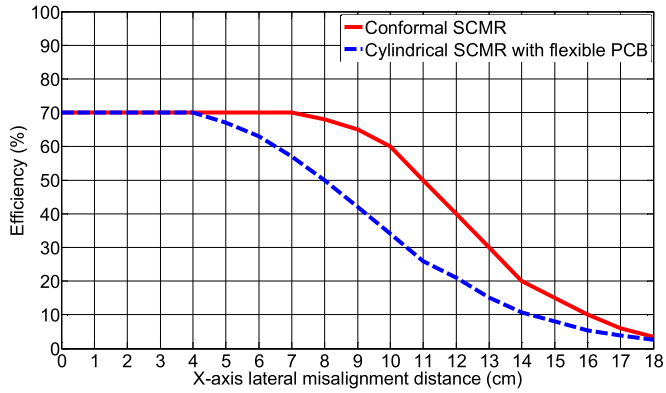

Fig. 20. Measured x-axis lateral misalignment results of conventional CSCMR and proposed cylindrical SCMR with flexible PCB.

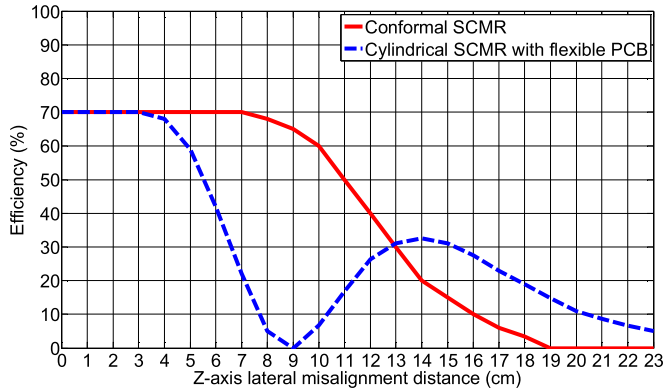

Fig. 21. Measured z-axis lateral misalignment results of conventional CSCMR and proposed cylindrical SCMR with flexible PCB.

efficiency of proposed cylindrical SCMR (see Fig. 20) stays approximately constant at 70% from 0 to 4 cm of lateral misalignment, and then gradually drops to almost zero from 4 to 18 cm of lateral misalignment. Therefore, conventional CSCMR has better performance in terms of x-axis lateral misalignment. This is expected as the cylindrical element in this case has smaller width in the x-axis than the conformal element.

For the z-axis lateral misalignment, the performance for conventional CSCMR (see Fig. 21) is identical to that of the x-axis lateral misalignment because of the symmetry in its square design for both transmitter and receiver. However, the efficiency of the proposed cylindrical SCMR (see Fig. 21) stays approximately constant at 70% from 0 cm to 3 cm of lateral misalignment, and then gradually drops to almost zero from 3 cm to 9 cm. From 9 cm to 14 cm the efficiency increases from 0% to 32.5% while surpassing the efficiency of CSCMR at 13 cm and starts decreasing again after 14 cm to almost zero at 23 cm. The null of the efficiency at 9 cm and the local maximum at 14 cm can be attributed to destructive and constructive addition of the magnetic fields at these distances, respectively.

In summary, conventional CSCMR provides better performance than the proposed cylindrical SCMR for both the x-axis and z-axis lateral misalignment. The lateral misalignment results were provided for completeness for this research. However, the proposed cylindrical SCMR design was specifically developed to address the problems of standard SCMR and conventional CSCMR for angular misalignment, for which it indeed provided significantly improved performance with no nulls in the efficiency.

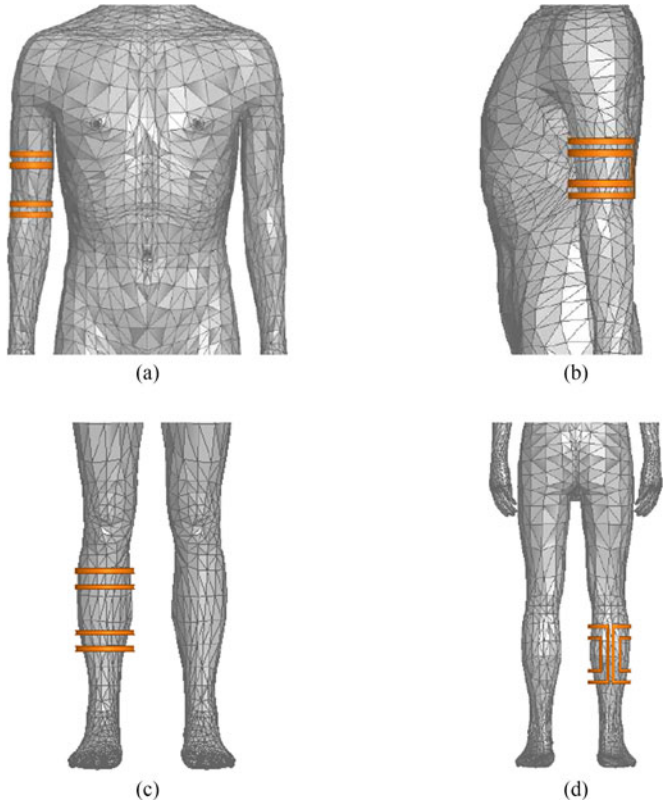

Fig. 22. Demonstration of wearable cylindrical SCMR in simulation.

IV. Wearable Applications

In previous sections, the conventional CSCMR and the proposed cylindrical SCMR were compared in terms of their misalignment sensitivity and it was concluded that the proposed cylindrical geometry is significantly less misalignment sensitive as it exhibits no nulls through the 360° of misalignment rotation. Specifically, the proposed cylindrical SCMR system with flexible PCB maintained approximately constant efficiency of 70% from 60° to 270° of misalignment angle, and exhibited an efficiency that varied from approximately 35% to 70% for misalignment angles between 0° to 60° and 270° to 360°, as shown in Fig. 17. In this section, the possible wearable applications of this proposed cylindrical topology are discussed.

Given the cylindrical geometry of the proposed SCMR system, the new models can easily be wrapped around a human's arm or leg while maintaining its shape and position, as shown in Fig. 22. A human body model that includes more than 300 parts of biological tissues was used. In this human body model, the materials of biological tissues are characterized by 28 sets of frequency-dependent relative permittivity ε_r and conductivity σ. This model is compatible with ANSYS HFSS and it was used in our simulations. Also, in order to show how this system actually works in future practical applications, the cylindrical system prototype with flexible PCB was placed on the arm and leg of a volunteer, as shown in Fig. 23. Such cylindrical elements

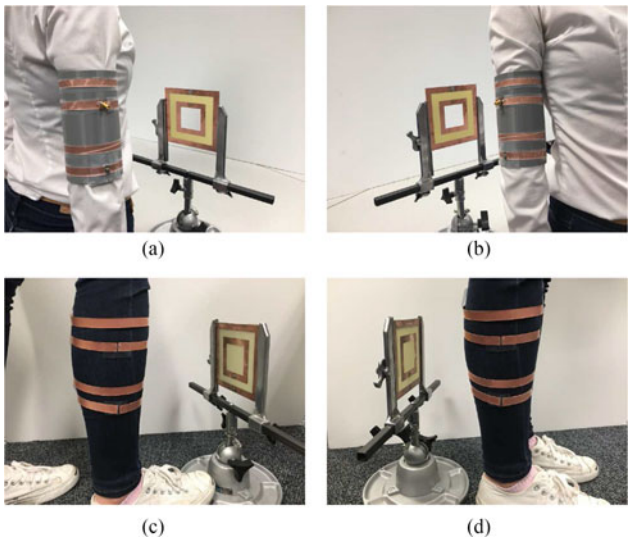

Fig. 23. Wearable cylindrical SCMR in measurement setup.

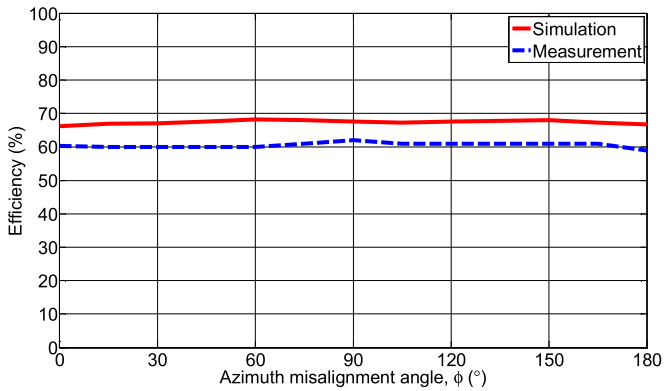

Fig. 24. Misalignment results of wearable cylindrical SCMR system from 0° to 180° (this angle range corresponds to angles 90° to 270° per the setup of Fig. 17).

can be implemented either on wearable devices that separate the elements from the skin using nonmetallic materials or they can be woven into the clothes (i.e., electronics woven in textiles). It is worth mentioning that in this wearable application, the transmitter is the conformal planar element and the receiver is the cylindrical element. For practical reasons, the volunteer rotates from facing the conformal transmitter as shown in Fig. 23(a) and (c) to the opposite way illustrated in Fig. 23(b) and (d), which is a 180° rotation. Given that only 180° rotation is needed here, the part of the cylindrical structure that is not complete can be avoided which will eliminate low efficiencies caused by the gap thereby enabling this wearable system to have high steady efficiencies through 180° of misalignment. For comparison purposes, the distance between the transmitter and receiver is kept the same with the system presented in the previous section. The following results are from the model being wrapped around the arm, as an example.

Fig. 24 illustrates the results from both simulation with human body in HFSS and measurement. Fig. 24 is a plot only showing 0° to 180° misalignment, as discussed previously in this section. In wearable situations, it is most practical to only measure 0° to 180° misalignment, with 0° being the volunteer facing the conformal elements, and 180° being the facing away from the conformal elements (see Fig. 23). With this setup and by facing the gap of the cylindrical loops toward the human body, we can avoid the angles that face this gap toward the conformal TX element, which yields lower efficiencies as shown in Fig. 17. In other words, Fig. 24 shows the efficiencies from 90° to 270° per the setup of Fig. 17, and this is the reason that the efficiency does not decrease at the beginning and end of Fig. 24. Since the cylindrical elements are wrapped around human arm, the performance of the system is affected by the properties of the human body, which are shown in Table III. Here, we only listed the four sets of the biological tissue properties that were most relevant to this specific placement, i.e., wrapping around the arm. During the simulation process, all of the properties in Table III are taken into consideration. Given that the material resistivity is the reciprocal value of the conductivity, the optimal design of the system will be different, according to (1)–(5). The simulated and measured results also show that the efficiency of this design in the wearable case (see Fig. 24) is approximately 10% lower than the efficiency of the same design in air (see Fig. 17).

TABLE III
MATERIAL PROPERTIES OF HUMAN BODY IN SIMULATION

	Permittivity	Conductivity
Blood	154.6	1.15
Bone	36.6	0.0925
Fatty tissue	9.726	0.032
Muscle	107.2	0.67

The purpose of this section is to demonstrate that the cylindrical system presented earlier provides misalignment insensitive performance also for wearable scenarios. Detailed investigation of such scenarios is beyond the scope of this paper and the optimization of the proposed cylindrical SCMR systems for wearable applications will be studied by future research. Furthermore, the safety of such wearable systems according to the relevant safety regulations will be studied in the future. The slight difference in efficiency between simulation and measurement is because the capacitors used in the prototype are not ideal as in simulation, therefore slightly affecting the performance of the system. The results of Fig. 24 clearly show that this cylindrical SCMR topology can be used as a wearable device, if direct contact with the skin is avoided.

The advantage of this system for wearable applications is that no matter which way a person turns, this device can always transfer or receive power or data as needed, without concerns of the orientation. One good example of the application would be for a patient lying in bed in a hospital. The conformal transmitter (receiver) could be set under the bed while the cylindrical receiver (transmitter) is wrapped around the patient's arm or leg. With this setup, no matter which way the patient is turning, power or data can always be wirelessly transferred. As a result, using the wearable cylindrical system can be very convenient for a patient by eliminating all the wires whilst maintaining a high efficiency.

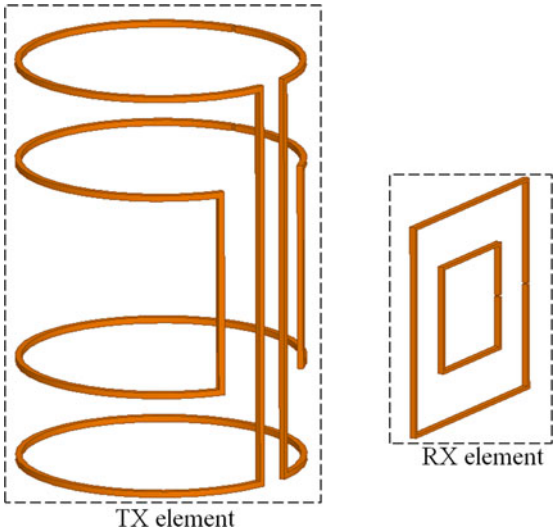

Fig. 25. Optimized cylindrical SCMR system based on wire elements.

V. Optimizing Cylindrical SCMR

Previously, it was mentioned that in our designs, the geometries of the cylindrical elements are kept consistent with the geometry of the CSCMR design in terms of the heights of the source loop and TX resonator. This was done to have a consistent comparison among all the designs, and to ensure that size differences did not contribute to differences in efficiency. However, this procedure results in the cylindrical elements not resonating at the maximum Q-factor frequency, as shown in Figs. 9 and 15, hence the highest possible efficiency was not achieved. In order to optimize the cylindrical SCMR system to achieve higher efficiency, in this section, we design a cylindrical SCMR system based on wire elements for the TX and RX elements with maximum Q-factor at the operating frequency of 27.12 MHz.

As was shown in Fig. 9, the maximum Q-factor frequency of the cylindrical element is larger than the operating frequency. In order to optimize the efficiency, the size of the cylindrical element has to be larger for the Q-factor to resonate at a lower frequency. Using simulation tools, we found out that when the cylindrical TX element is 1.9 times larger than the original size while the conformal RX element stays the same, the frequency of the maximum Q-factor of both elements coincide at 27.12 MHz.

The optimized cylindrical SCMR system is shown in Fig. 25 and its specifications are as follows. The radius of the cylindrical elements is 76 mm. The height of the TX resonator is 218.5 mm. The height of the source loop is 109.25 mm. The conformal RX element is the same with the design of Section III-B, where the height of RX resonator is 115 mm and the height of load loop is 57.5 mm. The distance between the outer surface of the TX and RX element is 70 mm. The capacitors for TX and RX resonators are 54 pF and 100 pF, respectively. This system design results in the same maximum Q-factor frequency of 27.2 MHz for both TX and RX elements, as it can be seen in Fig. 26.

Given that in this design both TX and RX resonators achieve their maximum Q-factor at the same frequency, this design should achieve higher efficiency than the previous design in Section III-B. Fig. 27 confirms this, as it shows that the

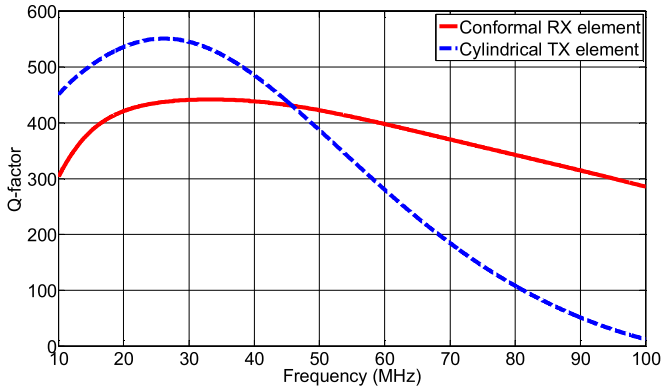

Fig. 26. Simulated Q-factor of elements of optimized cylindrical SCMR system based on wire elements.

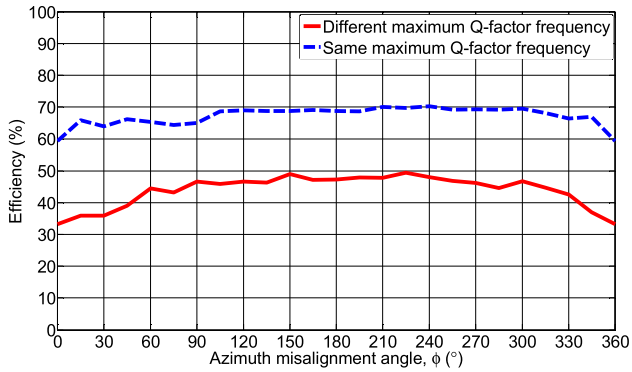

Fig. 27. Comparison of simulated misalignment results of proposed and optimized cylindrical SCMR systems based on wire elements.

efficiency of the design presented here (that has TX and RX resonators exhibiting maximum Q-factors at 27.12 MHz) is significantly larger than the efficiency of the design in Section III-B (that has TX and RX resonators that do not both exhibit maximum Q-factors at 27.12 MHz). Specifically, the efficiency of the optimized cylindrical SCMR system is approximately 20% larger than the efficiency of the design in Section III-B over the entire 360° of misalignment rotation.

This paper aimed to present a novel structure that generates no nulls throughout the 360° misalignment rotation and this was achieved by both the optimized design of this section (with TX and RX resonators that exhibit maximum Q-factors at 27.12 MHz) as well the design of Section III-B (with TX and RX resonators that have the same height). It was also shown that optimization of the efficiency can be done by changing the size of the cylindrical element. Before this section, the heights of the TX and RX resonators of all designs were kept the same to avoid comparing elements with different heights and introducing another variable in the comparison of the designs that could lead to uncertainty about their performance comparison.

VI. Conclusion

This paper proposed, for the first time, a novel structure of a WPT system based on SCMR principle that has no nulls throughout the 360° misalignment rotation, which is a significant improvement over the standard SCMR systems.

First, the efficiency of conventional CSCMR system was examined for all azimuth misalignment angles. It was shown that its efficiency stays approximately 70% for misalignment angles of 0° to 60°, 120° to 240°, and 300° to 360°. Also, since no magnetic flux can be coupled when the transmitter is perpendicular to the receiver, the efficiency drops from 70% to 0% from 60° to 90°, 120° to 90°, 240° to 270°, and 300° to 270°. Therefore, even though conventional CSCMR provides significant space savings compared to the standard SCMR [21], it still exhibits efficiency nulls when the transmitter and receiver are perpendicular to each other.

Second, the efficiency of the proposed cylindrical SCMR system made by copper wire was studied. It was shown that the efficiency of this system exhibited no nulls for the entire 360° misalignment rotation. Specifically, the efficiency varies from 30% to 40% throughout the 360° misalignment rotation. This demonstrated that the proposed SCMR cylindrical geometry is indeed significantly less misalignment sensitive in the azimuth plane. However, efficiencies for the wire model were not as high as the conventional CSCMR that was examined because the copper wire is very thin and exhibits high resistance.

Third, an improved version of this proposed topology was made and examined. Flexible PCBs were used instead of copper wire, and this change greatly enhanced the system's performance in terms of achieved efficiency. Specifically, the efficiency varies from 35% to 70% for 0° to 60°, and 270° to 360° misalignment angles. Also, the efficiency stays approximately constant at 70% from 60° to 270°. This proposed cylindrical SCMR system with flexible PCB not only exhibits no nulls for 360° rotation, but also generates efficiencies that are as high as the ones of conventional CSCMR.

Then, the lateral misalignment performances of conventional CSCMR and proposed cylindrical SCMR are compared. Under both x-axis and z-axis misalignment situations, the conventional CSCMR system out performs the proposed cylindrical SCMR system with more gradual efficiency decrease. These results suggest even though the proposed cylindrical SCMR has better angular misalignment performance, it has disadvantages. In practical applications, different system should be chosen depending on different needs.

Finally, given the misalignment insensitive performance of the flexible PCB cylindrical SCMR system, it was implemented into wearable scenarios. Considering its cylindrical shape, it is suitable for being wrapped around a human's arm or leg and still transmitting or receiving power and/or data while the person is moving around within a certain distance. This implementation of the proposed structure is suitable for various wireless applications where wires are inconvenient, such as hospital environments.

REFERENCES

[1] J. Lee and B. Han, "A bidirectional wireless power transfer EV charger using self-resonant PWM," *IEEE Trans. Power Electron.*, vol. 30, no.4, pp. 1784–1787, Apr. 2015.

[2] K. Finkenzeller RFID Handbook: Fundamentals and Applications in Contactless Smart Cards and Identification, 2nd ed. New York, NY, USA: Wiley, 2003, pp. 65–112.

[3] P. V. Nikitin, K. V. S Rao, and S. Lazar, "An overview of near field UHF RFID," in *Proc. RFID IEEE Int. Conf.*, Mar. 2007, pp. 167–174.

[4] D. Ahn and S. Hong, "Wireless power transmission with self-regulated output voltage for biomedical implant," *IEEE Trans. Ind. Electron.*, vol. 61, no. 5, pp. 2225–2235, May 2014.

[5] K. Chang-Gyun, S. Dong-Hyun, Y. Jung-Sik, P. Jong-Hu, and B. H. Cho, "Design of a contactless battery charger for cellular phone," *IEEE Trans. Ind. Electron.*, vol. 48, no. 6, pp. 1238–1247, Dec. 2001.

[6] A. Kurs, A. Karalis, R. Moffatt, J. D. Joannopoulos, P. Fisher, and M. Soljacic, "Wireless energy transfer via strongly coupled magnetic resonances," *Science*, vol. 317, pp. 83–85, 2007.

[7] A. Karalis, J. D. Joannopoulos, and M. Soljacic, "Efficient wireless nonradiative mid-range energy transfer", *Ann. Phys.*, vol. 323, pp. 34–48, Jan. 2008.

[8] B. L. Cannon, J. F. Hoburg, D. D. Stancil, and S. C. Goldstein, "Magnetic resonant coupling as a potential means for wireless power transfer to multiple small receivers," *IEEE Trans. Power Electron.*, vol. 24, no.7, pp. 1819–1825, Jul. 2009.

[9] O. Jonah and S. V. Georgakopoulos, "Wireless power transmission to sensors embedded in concrete via magnetic resonance," in *Proc. 2011 IEEE 12th Annu. Wireless Microw. Technol. Conf.*, Apr. 2011, pp. 1–6.

[10] S. G. Lee, H. Hoang, Y. H. Choi, and F. Bien, "Efficiency improvement for magnetic resonance based wireless power transfer with axial-misalignment," *Electron. Lett.*, vol. 48, no. 6, pp. 339–340, Mar. 15, 2012.

[11] W. Zhong and S. Y. R. Hui, "Auxiliary circuits for power flow control in multifrequency wireless power transfer systems with multiple receivers," *IEEE Trans. Power Electron.*, vol. 30, no.10, pp. 5902–5910, Oct. 2015.

[12] D. Ahn and S. Hong, "Effect of coupling between multiple transmitters or multiple receivers on wireless power transfer," *IEEE Trans. Ind. Electron.*, vol. 60, no. 7, pp. 2602–2613, Jul. 2013.

[13] K. Fotopoulou and B. W. Flynn, "Wireless power transfer in loosely coupled links: coil misalignment model," *IEEE Trans. Magn.*, vol. 47, no. 2, pp. 416–430, Feb. 2011.

[14] O. Jonah, S. V. Georgakopoulos, and M. M. Tentzeris, "Orientation insensitive power transfer by magnetic resonance for mobile devices," *IEEE Wireless Power Trans.*, pp. 5–8, May 15–16, 2013.

[15] W. Junhua, S. L Ho, W. N. Fu, and Sun Mingui, "Analytical design study of a novel witricity charger with lateral and angular misalignments for efficient wireless energy transmission," *IEEE Trans. Magn.*, vol. 47, no. 10, pp. 2616–2619, Oct. 2011.

[16] F. Zhang, S. A. Hackwoth, X. Liu, L. Chengliu, and S. Mingui, "Wireless power delivery for wearable sensors and implants in body sensor networks," in *Proc. 2010 IEEE Annu. Int. Conf. Eng. Medicine Biology Soc.*, Aug. 31–Sep. 4, 2010, pp. 692–695.

[17] A. Sample, D. Meyer, and J. Smith, "Analysis, experimental results and range adaptation of magnetically coupled resonators for wireless power transfer," *IEEE Trans. Ind. Electron.*, vol. 58, no. 2, pp. 544–554, Feb. 2011.

[18] W. Ng, C. Zhang, D. Lin, and S. Y. R. Hui, "Two- and three-dimensional omnidirectional wireless power transfer," *IEEE Trans. Power Electron.*, vol. 29, no.9, pp. 4470–4474, Sep. 2014.

[19] C. Zhang, D. Lin and S. Y. Hui, "Basic control principles of omnidirectional wireless power transfer," *IEEE Trans. Power Electron.*, vol. 31, no. 7, pp. 5215–5227, Jul. 2016.

[20] Z. Dang, Y. Cao and J. A. A. Qahouq, "Reconfigurable magnetic resonance-coupled wireless power transfer system," *IEEE Trans. Power Electron.*, vol. 30, no. 11, pp. 6057–6069, Nov. 2015.

[21] D. Liu, H. Hu and S. V. Georgakopoulos, "Misalignment sensitivity of strongly coupled wireless power transfer systems," *IEEE Trans. Power Electron.*, vol. 32, no. 7, pp. 5509–5519, Jul. 2017.

[22] O. Jonah and S.V. Georgakopoulos, "Wireless power transmission to sensors embedded in concrete via magnetic resonance," in *Proc. Wireless Microw. Technol. Conf.*, Apr. 18—19, 2011, pp. 1–6.

[23] O. Jonah, S. V. Georgakopoulos, and M. M. Tentzeris, "Optimal design parameters for wireless power transfer by resonance magnetic," *IEEE Antennas Wireless Propag. Lett.*, vol. 11, pp. 1390–1393, 2012.

[24] D. Daerhan, O. Jonah, H. Hu, S. V. Georgakopoulos and M. M. Tentzeris. "Novel highly-efficient and misalignment insensitive wireless power transfer systems utilizing strongly coupled magnetic resonance principles," in *Proc. IEEE Electron. Compon. Technol. Conf.*, May 27–30, 2014, pp. 759–762.

[25] H. Hu, S. Yao, K. Bao and S. V. Georgakopoulos, "Misalignment insensitive WPT with conformal SCMR systems," in *Proc IEEE Int. Symp. Antennas Propag.*, Jul. 19–24, 2015, pp. 117–118.

[26] Z. Yan, Y. Li, C. Zhang and Q. Yang "Influence factors analysis and improvement method on efficiency of wireless power transfer via coupled magnetic resonance," *IEEE Trans. Magn.*, vol. 50, no. 4, Apr. 2014, Art. no. 4004204.
[27] H. Hu and S. V. Georgakopoulos, "Multiband and broadband wireless power transfer systems using the conformal strongly coupled magnetic resonance method," *IEEE Trans. Ind. Electron.*, vol. 64, no. 5, pp. 3595–3607, May 2017.
[28] C. A. Balanis *Antenna Theory*, 3rd ed. Hoboken, NJ, USA: Wiley, 2005.
[29] 2018. [Online]. Available: http://www.ansys.com/Products/Electronics/ANSYS-HFSS.
[30] 2018. [Online]. Available: http://resource.ansys.com/Products/Simulation+Technology/Electronics/RF+&+Microwave/ANSYS+DesignerRF/Features/ANSYS+Nexxim+Circuit+Solver+Technology+ANSYS+DesignerRF
[31] D. M. Pozar *Microwave Engineering*, 4th ed. Hoboken, NJ, USA: Wiley, 2011.
[32] Awai and T. Ishizaki, "Transferred power and efficiency of a couple-dresonator WPT system," in *Proc. IEEE MTT-S Int. Microw. Workshop Series Innov. Wireless Power Transmiss., Technol., Syst., Appl.*, May 2012, pp. 105–108.
[33] D. Ahn and S. Hong, "A transmitter or a receiver consisting of two strongly coupled resonators for enhanced resonant coupling in wireless power transfer," *IEEE Trans. Ind. Electron.*, vol. 61, no. 3, pp. 1193–1203, Mar. 2014.

Daerhan Liu (S'13) received the B.S. degree in electrical engineering from the University of Science and Technology Beijing, Beijing, China, in 2011, and the M.S. degree in electrical engineering from Florida International University, Miami, FL, USA, in 2013, where he is currently working toward the Ph.D. degree at the Department of Electrical and Computer Engineering.

He is a Research Assistant with the ElectroMagnetic Laboratory, Florida International University. His research interests include wireless powering of wearable and implantable devices, and novel wireless battery-less sensors.

Stavros V. Georgakopoulos (S'93–M'02–SM'11) received the Diploma in electrical engineering from the University of Patras, Patras, Greece, in June 1996, the M.S. degree in electrical engineering, and the Ph. D. degree in electrical engineering both from Arizona State University (ASU), Tempe, AZ, USA, in 1998, and 2001, respectively.

From 2001–2007, he held a position as Principal Engineer with SV Microwave, Inc. Since 2007, he has been with the Department of Electrical and Computer Engineering, Florida International University, Miami, FL, USA, where he is currently an Associate Professor. His current research interests include wireless powering of portable, wearable, and implantable devices, novel antennas, and wireless sensors.

Dr. Georgakopoulos was the recipient of the 2015 FIU President's Council Worlds Ahead Faculty Award, which is the highest honor FIU extends to a faculty member for excelling in research, teaching, mentorship and service. He serves as an Associate Editor for the IEEE TRANSACTIONS ON ANTENNAS AND PROPAGATION (2013–present).